

Tunable Circular Dichroism of Achiral Graphene Plasmonic Structures

Tiankun Wang¹ · Yongkai Wang¹ · Lina Luo¹ ·
Li Wang¹ · Zhongyue Zhang¹

Received: 12 January 2016 / Accepted: 6 July 2016 / Published online: 18 July 2016
© Springer Science+Business Media New York 2016

Abstract Graphene bilayered split rings (BSRs) are proposed to generate tunable circular dichroism (CD). BSRs with traditional materials do not elicit the CD effect because of C_4 symmetry. By contrast, BSRs with graphene can achieve the CD effect by varying the Fermi energy of each part of the split rings. The CD signal can be reversed from positive to negative or vice versa by exchanging the Fermi energy. CD effects can also be tuned by varying the Fermi energies of the different parts. This phenomenon indicates that the chirality of BSRs gradually change as the Fermi energy varies. This concept provides a method to change chirality and dynamically vary the CD effect without rebuilding the structures.

Keywords Bilayered split ring · Graphene · Circular dichroism · Plasmonics

Introduction

Chiral structures elicit different optical responses, such as circular dichroism (CD), under left circularly polarized (LCP) and right circularly polarized (RCP) light illumination [1, 2]. Novel structures have been designed to obtain a CD effect or to investigate the mechanism of CD effects because these effects of chiral structures are associated with biological monitoring, analytical chemistry, and plasmonic sensing [3–10].

Planar achiral structures generate CD effects under oblique illumination [3–5]. Under this condition, electric dipoles in different parts of planar achiral structures are not parallel, and phase differences are observed between them; thus, CD effects occur. Three-dimensional (3D) chiral structures, such as helix and layer-by-layer structures, also cause strong CD effects [6–11]. In addition to electric dipoles, magnetic dipoles are excited by antiparallel current on two layers of helix [6, 7] and layer-by-layer structures [8–10]. The CD effect of different nanostructures can be explained by a Born–Kuhn configuration [11], as a consequence, the twisted electric dipoles in nanostructures and the phase between them induce the CD effect.

Researchers vary structural parameters and redesign structures to tune the CD effects of various structures. However, the CD effects of traditional structures cannot be controlled dynamically. With single-layer carbon atoms gathered in a honeycomb lattice, graphene provides unique optical properties beneficial for electronic, structural, and transport applications [12–16]. Permittivity functions can be tuned by external gate voltages (Fermi energy of graphene) [12–15]. With these advantages, graphene is considered as a promising candidate of plasmonic materials to fabricate new-generation chiral structures. CD effects can be tuned by utilizing external gate voltages rather than by rebuilding structures in traditional materials.

In this study, a 3D array of bilayered split rings (BSRs) in graphene is proposed to generate CD effects. The structure of BSR is achiral. The transmissions of BSRs under circular polarized light illumination are controlled. The CD effects are generated by varying the Fermi energy of graphene by constantly changing the gate voltage of graphene. The CD effects can be inverted by exchanging the gate voltages of split rings. The CD effects can also be dynamically tuned by

✉ Zhongyue Zhang
zyzhang@snnu.edu.cn

¹ School of Physics and Information Technology, Shaanxi Normal University, Xi'an 710062, China

varying the gate voltages of split rings without changing the structural parameters.

Structure and Computational Method

Figure 1 shows the proposed 3D arrays of BSRs. The BSR is composed of two layers of separated broken rings [Fig. 1b]. These broken rings are named TOP₁, TOP₂, BOTTOM₁, and BOTTOM₂. The outer radius (R) and inner radius (r) of the rings in each broken ring are 40 and 30 nm, respectively. The distance (d) between two layers is 10 nm, the thickness of the graphene layer is 0.5 nm, and the periodic constant L is 150 nm. In all the calculations, V_{top1} and V_{top2} are equal to 0.9 and 0.5 eV, respectively. The Fermi energies of the two bottom parts can be tuned by varying the gate voltages V_{bottom1} and V_{bottom2} . The conductivity of graphene is a function of the frequency of incident light and computed within the local random phase approximation [12–15].

$$\sigma(\omega) = \frac{2ie^2k_B T}{\pi\hbar^2(\omega + i\tau^{-1})} \ln \left[2\cosh \left(\frac{E_f}{2k_B T} \right) \right] + \frac{e^2}{4\hbar} \left\{ \frac{1}{2} + \frac{1}{\pi} \arctan \left(\frac{\hbar\omega - 2E_f}{2k_B T} \right) - \frac{i}{2\pi} \ln \left[\frac{(\hbar\omega + 2E_f)^2}{(\hbar\omega - 2E_f)^2 + (2k_B T)^2} \right] \right\} \quad (1)$$

where e , \hbar , k_B , and E_f correspond to the electron charge, reduced Planck constant, Boltzmann constant, and Fermi energy (gate voltage), respectively. The carrier relaxation $\tau = \frac{\mu E_f}{ev_F^2}$, v_F is Fermi velocity, and μ is the measured DC mobility, $\mu = 10,000 \text{ cm}^2/\text{V}$ [12, 16]. In our study, Eq. 1 is simulated at $T = 300 \text{ K}$, and $k_B \times T$ refers to temperature energy. The first term in Eq. 1 corresponds to intraband electron–photon scattering processes. The second term represents the interband transition contribution. For the second term, the function of arctangent is a step function. The expression shows that the interband contribution becomes dominant at a frequency of

$\omega > E_f$ because of the absence of a gap between conduction and valence bands. At $\omega < E_f$, the opposite case is evident; likewise, the intraband contribution is dominant [13, 14].

We performed numerical simulations by using the commercial finite element method software COMSOL Multiphysics. In the simulations, LCP and RCP normally illuminated the structure. Two perfectly matched layers were located at both ends of the whole model, and the absorbing boundary conditions were applied to the z -direction. Periodic boundary conditions were applied to the x - and y -directions. Transmittance is defined as $T = P_{\text{out}}/P_{\text{in}}$, which is the ratio of output power to incident power. If we use a “+” (“–”) subscript of RCP (LCP) light, T_{+} (T_{-}) represents the transmittance of RCP (LCP) light. Then, the CD effect is defined as $\Delta T = T_{+} - T_{-}$ [17, 18].

Numerical Results and Discussions

Figure 2a shows the transmission spectra of BSRs under LCP and RCP illumination. The Fermi energies of the bottom layers V_{bottom1} and V_{bottom2} are 0.9 and 0.5 eV, respectively. Five evident resonant modes, namely, $\lambda_{\text{I}} = 8.20 \mu\text{m}$, $\lambda_{\text{II}} = 7.12 \mu\text{m}$, $\lambda_{\text{III}} = 6.16 \mu\text{m}$, $\lambda_{\text{IV}} = 5.13 \mu\text{m}$, and $\lambda_{\text{V}} = 4.84 \mu\text{m}$, are observed in the transmission spectra from 4.0 to 9.0 μm . These modes are labeled as I, II, III, IV, and V, respectively. The CD effects are also observed in these five resonant modes [Fig. 2b].

We examined the distributions of the surface current density of BSRs at resonant modes to understand the CD mechanism of BSRs in graphene. Figure 3 shows the distributions of the surface current density of BSRs under RCP illumination at the resonant wavelengths. Figure 3a, d, g, j, m shows the surface current density of the top layer of BSRs at the five resonant wavelengths. The pink dotted arrows represent the equivalent electric dipole moments of TOP₁ or TOP₂.

Fig. 1 **a** Schematic model of three-dimensional array of chiral bilayered split rings in graphene under LCP and RCP and **b** is unit cell structure of our design

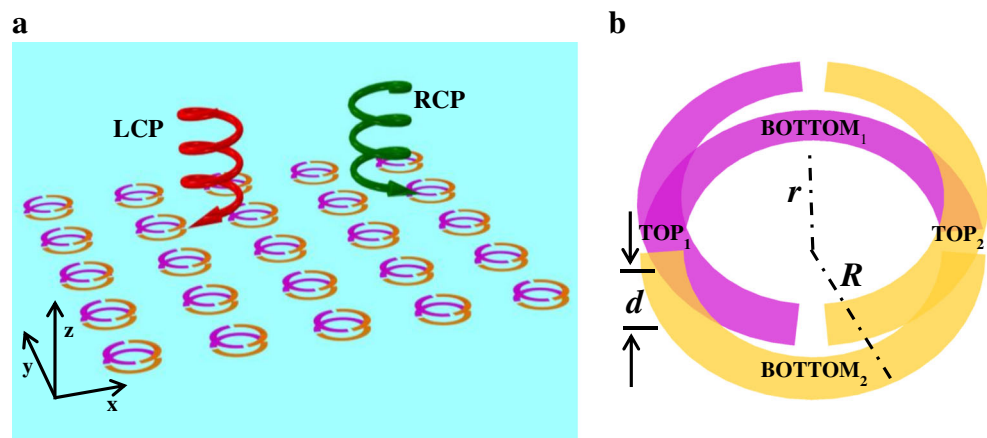


Fig. 2 **a** Simulated transmission spectra of LCP and RCP light for the CBSR; **b** The different transmittance spectra of CBSR with $V_{top1} = 0.9$ eV, $V_{top2} = 0.5$ eV, $V_{bottom1} = 0.9$ eV, and $V_{bottom2} = 0.5$ eV

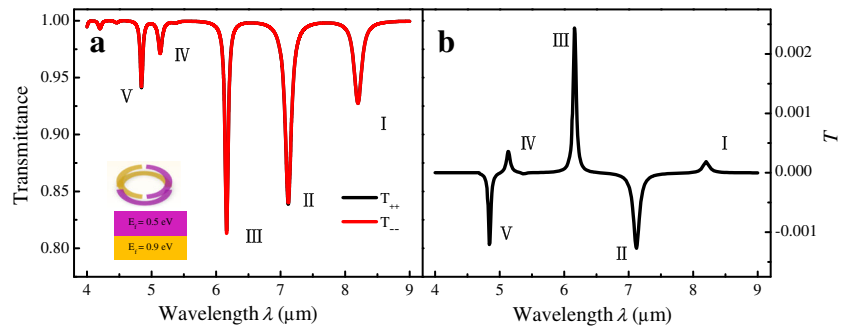


Figure 3b, e, h, k, n reveals the surface current density of the bottom layer of the BSR at five resonant wavelengths. The blue-dotted arrows represent the equivalent electric dipole moments of BOTTOM₁ or BOTTOM₂.

At $\lambda_I = 8.20$ μm , the main currents are detected in TOP₂ and BOTTOM₂ [Fig. 3a, b]. In TOP₂, the currents flow from the middle part to the two ends, which form the effective dipole electron oscillation P_{IT} . In BOTTOM₂, the currents also flow from the middle part to the two ends, which form P_{IB} . P_{IT} in TOP₂ and P_{IB} in BOTTOM₂ constitute a bonding mode [Fig. 3c]. At $\lambda_{II} = 7.12$ μm , the main currents also appear in TOP₂ and BOTTOM₂ [Figs. 3d, e]. In TOP₂, the currents flow from the middle part to the two ends, which form P_{IT} . In BOTTOM₂, the currents flow from the two ends to the middle part, which form P_{IB} . P_{IT} and P_{IB} form an antibonding mode [Fig. 3f]. At $\lambda_{III} = 6.16$ μm , $P_{III T}$ in TOP₁ and $P_{III B}$ in BOTTOM₁ constitute a bonding mode

[Fig. 3i]. At $\lambda_V = 4.84$ μm , P_{VT} in TOP₁ and P_{VB} in BOTTOM₁ form an antibonding mode [Fig. 3o]. In TOP₂ and BOTTOM₂, a strong current is associated with the coupling with TOP₁ and BOTTOM₁, respectively. At $\lambda_{IV} = 5.13$ μm , three kinds of currents are observed in TOP₂ and BOTTOM₂ [Fig. 3j, k]. $P_{IV T}$ in TOP₂ and $P_{IV B}$ in BOTTOM₂ also constitute a bonding mode [Fig. 3l].

The chirality of BSR can be tuned by the exchange in the gate voltages of the different parts of BSR because the dielectric functions of graphene depend on their gate voltages. Figure 4 shows the CD spectra of BSRs with $V_{bottom1} = 0.5$ eV, $V_{bottom2} = 0.9$ eV, and $V_{bottom1} = 0.9$ eV, $V_{bottom2} = 0.5$ eV. The CD effects evidently occur at the resonant wavelengths. A negative CD signal occurs when the gate voltages are exchanged at the wavelength with a positive CD signal. Thus, the BSR changes to its enantiomer when the gate voltage is

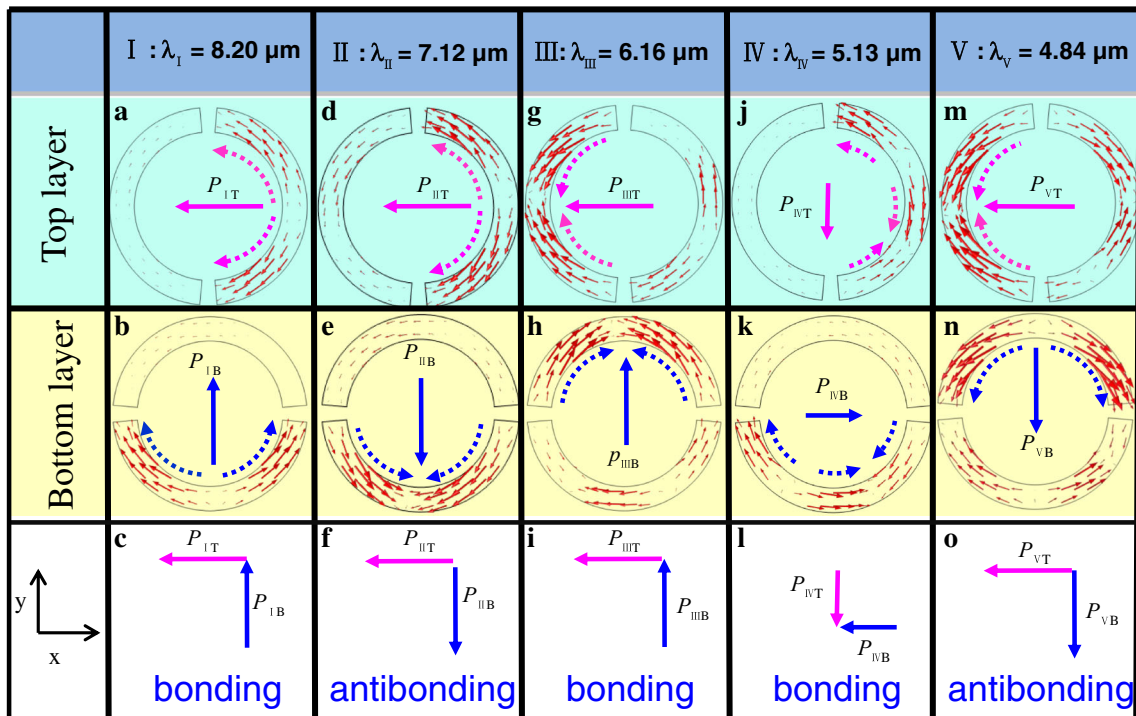


Fig. 3 The effective dipole electron oscillation of surface current of the BSR and the resonant mode at resonant modes

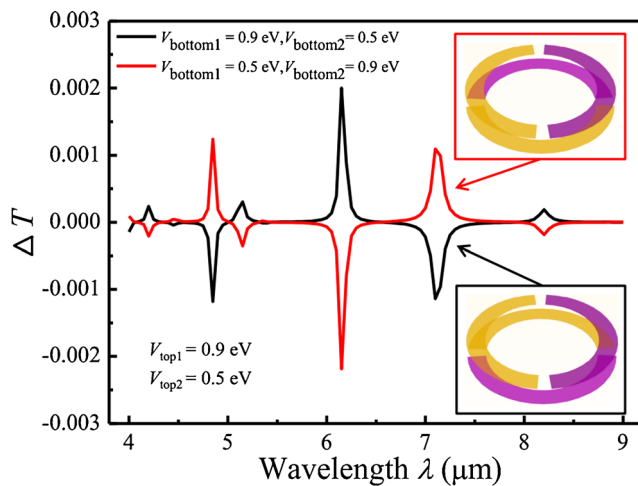


Fig. 4 Simulated difference of transmittance of the BSR with $V_{\text{top1}} = 0.9$ eV, $V_{\text{top2}} = 0.5$ eV, $V_{\text{bottom1}} = 0.9$ eV, and $V_{\text{bottom2}} = 0.5$ eV (black line); $V_{\text{top1}} = 0.9$ eV, $V_{\text{top2}} = 0.5$ eV, $V_{\text{bottom1}} = 0.5$ eV, and $V_{\text{bottom2}} = 0.9$ eV (red line)

exchanged. This phenomenon confirms that we can change the chirality of BSR by tuning the Fermi energy of graphene rather than by rebuilding the structure.

Variations in the gate voltage applied to different parts likely influence the CD effect of the BSRs. We systematically changed the Fermi energies of four parts to investigate the CD effect of the BSRs. Figure 5a illustrates the simulated CD effect of BSRs with $V_{\text{bottom2}} = 0.5, 0.6, 0.7, 0.8,$ and 0.9 eV, at a fixed $V_{\text{bottom1}} = 0.9$ eV. The CD effect is evident at the five resonant wavelengths. As V_{bottom2} increases, modes I, II, IV, and V exhibit an obvious blue shift. By contrast, mode III manifests a slight blue shift. The CD signal is disappeared at $V_{\text{bottom1}} = V_{\text{bottom2}} = 0.9$ eV. Figure 5b shows the simulated CD effect of BSRs with $V_{\text{bottom2}} = 0.5, 0.6, 0.7, 0.8,$ and 0.9 eV, at a fixed $V_{\text{bottom1}} = 0.7$ eV. As V_{bottom2} increases, modes I, II, IV, and V exhibit an obvious blue shift. Mode III displays a slight blue shift when $V_{\text{bottom1}} > V_{\text{bottom2}}$. Modes I, III, IV, and V manifest an obvious blue shift and mode II shows a slight blue shift when $V_{\text{bottom1}} < V_{\text{bottom2}}$. The CD signal disappears when $V_{\text{bottom1}} = V_{\text{bottom2}} = 0.7$ eV. Figure 5(c) illustrates the simulated CD effect of BSRs with $V_{\text{bottom2}} = 0.5, 0.6, 0.7, 0.8,$ and 0.9 eV, at a fixed $V_{\text{bottom1}} = 0.5$ eV. As V_{bottom2} increases, modes I, III, IV, and V manifest an obvious blue shift, and mode II displays a slight blue shift. The CD signal disappears when $V_{\text{bottom1}} = V_{\text{bottom2}} = 0.5$ eV. The behavior of the blue shift in Fig. 5a–c can be clarified as the resonance condition of surface plasmons. The resonant frequency f_r of the surface plasmons can be approximately described as a function of Fermi energy $\sqrt{E_f}$ because the wave vector of the surface plasmons along the graphene layer is expressed as $k_{\text{spp}} \propto \frac{\hbar f_r^2}{2\alpha_0 E_f c}$ [19], where $\alpha_0 = \frac{e^2}{\hbar c}$ is the fine

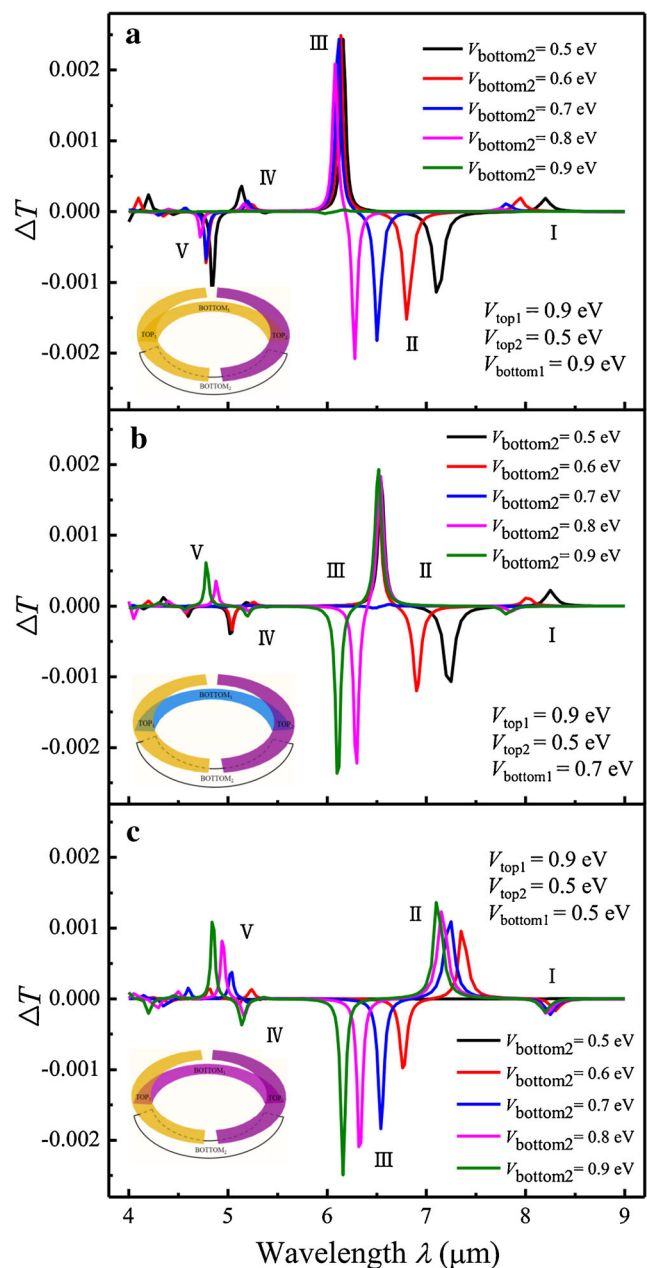


Fig. 5 Simulated difference of transmittance of the BSR with different Fermi energy on bottom layer

structure constant, f_r is the resonant frequency, and c is the speed of light in a vacuum. We obtained the function of $\lambda = \frac{c}{f_r} \propto \frac{c}{\sqrt{E_f}}$. In Fig. 5a, the changes in V_{bottom2} affect modes I, II, IV, and V because these modes are attributed to the electron oscillation in BOTTOM₂. Conversely, mode III is attributed to the electron oscillation in BOTTOM₁. Minor changes in the surrounding environment lead to the slight shift of mode III. The evident blue shift in Fig. 5b, c is also caused by the electron oscillation in BOTTOM₂ and the slight blue shift is due to the electron oscillation in BOTTOM₁.

Conclusion

The CD effects are not observed under circular polarized light illumination of the symmetric structure in traditional materials. In this study, symmetric BSRs are proposed. By contrast, BSRs can induce a CD effect when these rings are composed of graphene, and different parts of BSRs are formed by different Fermi energies. Furthermore, a positive (negative) CD signal can be reversed to a negative (positive) signal as Fermi energies of the different parts vary. CD signals can also be dynamically tuned by varying the Fermi energies of different parts of the BSRs. The dynamic tuning of the CD signal indicates that the chirality of BSRs is altered when the CD signal changes from positive to negative or vice versa. Thus, enantiomers can be obtained without rebuilding structures. Moreover, the mode of the required CD signal can be conveniently tuned.

Acknowledgments This work was supported by National Natural Foundation of China (Grant No. 61575117), the Fundamental Research Funds for the Central Universities (GK201303007), excellent doctor degree dissertation of Shaanxi Normal University (X2014YB08), and Innovation Funds of Graduate Programs of Shaanxi Normal University (2016CSZ013).

References

- Hentschel M, Wu L, Schäferling M, Bai P, Li EP, Giessen H (2012) Optical properties of chiral three-dimensional plasmonic oligomers at the onset of charge-transfer plasmons. *ACS Nano* 6(11):10355–10365
- Cui Y, Kang L, Lan S, Rodrigues S, Cai W (2014) Giant chiral optical response from a twisted-arc metamaterial. *Nano Lett* 14(2):1021–1025
- Plum E, Liu XX, Fedotov VA, Chen Y, Tsai DP, Zheludev NI (2009) Metamaterials: optical activity without chirality. *Phys Rev Lett* 102(11):113902
- Zhang W, Wang Y, Wen X, Zhang Z (2015) Giant circular dichroism induced by silver nanocuboid heterodimers. *Appl Opt* 54(31):9359–9363
- Cao T, Wei C, Zhang L (2014) Modeling of multi-band circular dichroism using metal/dielectric/metal achiral metamaterials. *Optical Materials Express* 4(8):1526–1534
- Gansel JK, Wegener M, Burger S, Linden S (2010) Gold helix photonic metamaterials: a numerical parameter study. *Opt Express* 18(2):1059–1069
- Zhang ZY, Zhao YP (2011) The visible extinction peaks of Ag nanohelices: a periodic effective dipole model. *Appl Phys Lett* 98(8):083102
- Wu S, Xu S, Zhang Y, Wu Y, Jiang J, Wang Q, Zhu Y (2014) Asymmetric transmission and optical rotation of a quasi-3D asymmetric metallic structure. *Opt Lett* 39(22):6426–6429
- Wu L, Yang Z, Cheng Y, Lu Z, Zhang P, Zhao M, Duan J (2013) Electromagnetic manifestation of chirality in layer-by-layer chiral metamaterials. *Opt Express* 21(5):5239–5246
- Cao T, Zhang L, Simpson RE, Wei C, Cryan MJ (2013) Strongly tunable circular dichroism in gammadion chiral phase-change metamaterials. *Opt Express* 21(23):27841–27851
- Yin X, Schäferling M, Metzger B, Giessen H (2013) Interpreting chiral nanophotonic spectra: the plasmonic born–Kuhn model. *Nano Lett* 13(12):6238–6243
- Singh V, Joung D, Zhai L, Das S, Khondaker SI, Seal S (2011) Graphene based materials: past, present and future. *Prog Mater Sci* 56(8):1178–1271
- Ligato N, Cupolillo A, Sindona A, Riccardi P, Pisarra M, Caputi LS (2014) A comparative study of the plasmonic properties of graphene on lattice-matched and lattice-mismatched Ni surfaces. *Surf Sci* 626:40–43
- Fürst JA, Pedersen JG, Flindt C, Mortensen NA, Brandbyge M, Pedersen TG, Jauho AP (2009) Electronic properties of graphene antidot lattices. *New J Phys* 11(9):095020
- Weser M, Rehder Y, Horn K, Sicot M, Fonin M, Preobrajenski AB, Dedkov YS (2010) Induced magnetism of carbon atoms at the graphene/Ni (111) interface. *Appl Phys Lett* 96(1):012504
- Yuan S, Roldán R, Jauho AP, Katsnelson MI (2013) Electronic properties of disordered graphene antidot lattices. *Phys Rev B* 87(8):085430
- Cheng H, Chen S, Yu P, Duan X, Xie B, Tian J (2013) Dynamically tunable plasmonically induced transparency in periodically patterned graphene nanostrips. *Appl Phys Lett* 103(20):203112
- Lu H, Zeng C, Zhang Q, Liu X, Hossain MM, Reineck P, Gu M (2015) Graphene-based active slow surface plasmon polaritons. *Scientific reports*. 5.
- Carrasco E, Tamagnone M, Mosig JR, Low T, Perruisseau-Carrier J (2015) Gate-controlled mid-infrared light bending with aperiodic graphene nanoribbons array. *Nanotechnology* 26(13):134002